Supporting Information for "History-dependent volcanic ground deformation from broad-spectrum viscoelastic rheology around magma reservoirs"

Yang Liao[1], Leif Karlstrom[2], Brittany A. Erickson[2,3]

[1]Department of Geology and Geophysics, Woods Hole Oceanographic Institution

[2]Department of Earth Sciences, University of Oregon

[3]Department of Computer Science, University of Oregon

Contents of this file

Introduction

This supplementary material provides mathematical derivations and descriptions of the numerical schemes used for generating the results shown in the main text. Supplemental figures support the results in the main text.

Text S1. Quantitative derivations

Model setup, temperature profile and temperature-dependent rheology

The geometry of the model is shown in Figure 1a. The magma chamber is a spherical cavity with radius r_o and depth d from the surface. The magma chamber is subjected to a pressure

---

₀

:

forcing that results in crustal deformation, stresses, and surface uplift. The response of the crust to the given pressure forcing depends on its rheology, which we assume to be viscoelastic (Maxwell model), with uniform elastic rigidity and a temperature-dependent shear viscosity. We consider the system to be an infinite domain while solving for the temperature and crustal stresses, then correct the full-space solution to satisfy stress free boundary conditions on a flat interface (the Earth's surface). This allows us to obtain surface displacements as a first order approximation (we match boundary conditions at the free surface exactly but only approximately at the chamber, (McTigue, 1987)).

Spatial variation in viscosity is found by solving a steady state heat equation with spherical symmetry (a function of radial distance r, with $r_0 \leq r \leq d$), namely

$$\nabla^2 T = 0, \quad T(r_o) = T_{in}, \quad T(d) = T_{surface}, \tag{1}$$

where T_{in} is the chamber temperature and $T_{surface} = 0^o C$ is the temperature approximated for the radial distance of chamber depth. The solution to (1) is $T(r) = -T_{in}\frac{1}{d/r_o-1} + \frac{T_{in}}{r/ro-r/d}$, shown in Figure1A in the main text. The temperature gradient at the surface caused by the spherically symmetric temperature profile is $dT/dr|_{r=d} = -\frac{T_{in}}{d^2/r_o-d}$ and is a reasonable approximation of the expected magmatic geotherm above the chamber that includes a background vertical gradient (Del Negro et al., 2009), if the temperature gradient meets or exceeds the expected vertical gradient. Figure S1 shows the surface thermal gradient varying with chamber temperature and depth for two different chamber sizes. If the vertical gradient is $-20°C$/Km, a $1000°C$ chamber meets this requirement for depths shallower than 8km. In our study, examples are shown for a chamber with $1000°C$ at a depth of 5km.

We model spatially variable shear viscosity $\eta(r)$ as temperature dependent according to the Arrhenius formula (Del Negro et al., 2009)

$$\eta(r) = A_d e^{\frac{E}{RT(r)}} \tag{2}$$

where A_d is the Dorn parameter, E is the activation energy, and R is the Boltzmann constant. The viscosity increases away from the chamber with decreasing temperature (Figure1 A).

Constitutive relations for a Maxwell viscoelastic material with radial symmetry and including variable viscosity are

$$
\begin{aligned}
\dot{\sigma}_{rr} + \frac{\mu}{\eta(r)}\sigma_{rr} &= \frac{\mu K}{\eta(r)}\left(\frac{\partial u}{\partial r} + \frac{2u}{r}\right) + \left(K - \frac{2}{3}\mu\right)\left(\frac{\partial \dot{u}}{\partial r} + \frac{2\dot{u}}{r}\right) + 2\mu\frac{\partial \dot{u}}{\partial r}, \\
\dot{\sigma}_{\theta\theta} + \frac{\mu}{\eta(r)}\sigma_{\theta\theta} &= \frac{\mu K}{\eta(r)}\left(\frac{\partial u}{\partial r} + \frac{2u}{r}\right) + \left(K - \frac{2}{3}\mu\right)\left(\frac{\partial \dot{u}}{\partial r} + \frac{2\dot{u}}{r}\right) + 2\mu\frac{\dot{u}}{r}, \\
\dot{\sigma}_{\varphi\varphi} + \frac{\mu}{\eta(r)}\sigma_{\varphi\varphi} &= \frac{\mu K}{\eta(r)}\left(\frac{\partial u}{\partial r} + \frac{2u}{r}\right) + \left(K - \frac{2}{3}\mu\right)\left(\frac{\partial \dot{u}}{\partial r} + \frac{2\dot{u}}{r}\right) + 2\mu\frac{\dot{u}}{r},
\end{aligned} \tag{3}
$$

where $\sigma_{rr,\theta\theta,\varphi\varphi}(r,t)$ are the stresses in the crust, $u(r,t)$ is the radial displacement in the crust, and the overhead dot denotes the time derivative. The viscosity $\eta(r)$ is calculated from (2), K and μ are the elastic bulk modulus and instantaneous elastic shear modulus of the crust, here assumed as constant and uniform.

The crustal stresses and displacement are governed by quasistatic equilibrium equations, the explicit boundary condition at the chamber wall, and the implicit boundary condition infinitely far from the chamber, namely,

$$\nabla \cdot \sigma = 0, \quad \sigma_{rr}(r_o, t) = -P(t), \quad u(\infty, t) = 0, \tag{4}$$

where $P(t)$ is the given time-dependent chamber overpressure relative to an assumed lithostatic state (Dragoni & Magnanensi, 1989). For a given function $P(t)$, the constraints (4) lead to a unique solution containing approximate surface displacements.

Viscoelastic transfer function for radially varying temperature

:

The constitutive relations and boundary conditions (3)-(4) are cast in frequency space using Fourier transforms. Our model assumes that the temporal evolution of any (radially symmetric) quantity $f(t,r)$ can be represented in terms of its Fourier transform $\hat{f}(\omega, r)$, namely

$$f(t,r) = \int_{-\infty}^{\infty} \hat{f}(\omega, r) e^{i\omega t} d\omega, \tag{5}$$

where ω is the frequency with corresponding time period $\tau = 2\pi/\omega$. As all quantities considered in our study are real valued, $\hat{f}(-\omega)$ and $\hat{f}(\omega)$ are always complex conjugates, hence we consider only positive values for ω for the rest of this study. The special case $\omega = 0$ corresponds to the constant component in the time series and is chosen such that the displacement is 0 prior to chamber pressurization.

The transfer function between maximum vertical surface displacement and chamber over-pressure is defined as

$$\mathcal{H}\{u_z|P\} = \hat{u}_z/\hat{P} \tag{6}$$

where $\hat{u}_z$ and $\hat{P}$ are the Fourier transforms of the maximum vertical surface displacement and the chamber pressure. In this section we derive the transfer function starting from the viscoelastic rheology.

Applying the Fourier transform to the constitutive relation (3) leads to constitutive relations in frequency space that mimic an elastic medium,

$$\begin{aligned}
\hat{\sigma}_{rr} &= (K - \frac{2}{3}\mu^*)(\frac{\partial \hat{u}}{\partial r} + \frac{2\hat{u}}{r}) + 2\mu^* \frac{\partial \hat{u}}{\partial r}, \\
\hat{\sigma}_{\theta\theta} &= \hat{\sigma}_{\varphi\varphi} = (K - \frac{2}{3}\mu^*)(\frac{\partial \hat{u}}{\partial r} + \frac{2\hat{u}}{r}) + 2\mu^* \frac{\hat{u}}{r},
\end{aligned} \tag{7}$$

where $\hat{\sigma}_{rr,\theta\theta,\varphi\varphi}(r,\omega)$ and $\hat{u}(r,\omega)$ are the (complex) Fourier transforms of the stress components and radial displacement. The complex rigidity μ^* can be expressed in terms of the spatially varying Deborah number $De(r)$ and the spatially varying viscoelastic relaxation time $\eta(r)/\mu$,

given by

$$\mu^*(r,\omega) = \mu\frac{iDe(r)}{1+iDe(r)}, \quad De(r) = \omega\frac{\eta(r)}{\mu}. \tag{8}$$

We apply the equilibrium condition $\nabla \cdot \hat{\sigma} = 0$, which reduces to

$$\frac{1}{r^3}\frac{d}{dr}\left((K+\frac{4}{3}\mu^*)r^4\frac{d}{dr}\left(\frac{\hat{u}}{r}\right)\right) = 0,$$
$$(K+\frac{4}{3}\mu^*)r^4\frac{d}{dr}\left(\frac{\hat{u}}{r}\right) = C, \tag{9}$$

where complex constant C is a function of ω but independent of r. Eq (9) applies for both the elastic and viscoelastic cases with either uniform or non-uniform complex rigidity. For a magma chamber in elastic rock (i.e., no viscous relaxation of crust), the complex rigidity becomes a uniform real value $\mu^{*,el} = \mu$, which after substituting into (9) with implicit boundary condition $u/r(r \to \infty) = 0$ leads to

$$0 - \frac{\hat{u}^{el}}{r} = \frac{C^{el}}{K+\frac{4}{3}\mu}\int_r^\infty \frac{dx}{x^4}, \tag{10}$$

which, in combination with the constitutive relation (7), leads to the elastic solution

$$\hat{\sigma}_{rr}^{el}r^3 = \frac{4\mu}{3K+4\mu}C^{el}, \hat{u}^{el}r^2 = -\frac{1}{3K+4\mu}C^{el}, \tag{11}$$

derived in classical magma chamber models (McTigue, 1987; Dragoni & Magnanensi, 1989). We observe from the elastic solution (11) that the following relation holds for all r:

$$\frac{-r}{4\mu}\frac{\hat{\sigma}_{rr}^{el}}{\hat{u}^{el}} = 1, \tag{12}$$

which shows that the stress and displacement are always in phase and proportional — a characteristic of the elastic domain with radial symmetry.

To obtain surface displacements, we assume that the chamber is sufficiently deep $(d \gtrsim r_o)$ so that a simple correction for stress free conditions on the surface approximates the true boundary conditions (McTigue, 1987). The Fourier transform of the maximum vertical ground deforma-

:

tion for a spherical chamber $\hat{u}_z^{el}$ in an elastic halfspace can then be approximated as

$$\hat{u}_z^{el} = \frac{\hat{P}r_o^3}{\mu}\frac{1}{d^2}(1 - \nu), \tag{13}$$

where $\hat{P}$ is the Fourier transform of the chamber's overpressure $P(t)$, and ν is the Poisson's ratio of the elastic crust. The elastic case corresponds to the transfer function as defined in the main text, between the maximum vertical surface displacement and chamber overpressure

$$\mathcal{H}\{u_z^{el}|P\} = \frac{r_o^3}{\mu}\frac{1}{d^2}(1 - \nu). \tag{14}$$

The viscoelastic case now follows from the elastic case through the well known 'Correspondence Principal' (Fung, 1965) where μ^* is complex-valued and varies with r. Assuming the same implicit boundary condition, we obtain

$$0 - \frac{\hat{u}}{r} = C \int_r^\infty \frac{dx}{x^4(K + \frac{4}{3}\mu^*(x))}, \tag{15}$$

which leads to

$$\begin{aligned}
\hat{u} &= -Cr \int_r^\infty \frac{dx}{x^4(K + \frac{4}{3}\mu^*(x))} \\
\hat{\sigma} &= \frac{C}{r^3}\left(1 - 3Kr^3 \int_r^\infty \frac{dx}{x^4(K + \frac{4}{3}\mu^*(x))}\right).
\end{aligned} \tag{16}$$

The relation in (16) describes displacement and stress in an infinite viscoelastic domain. We find that with decreasing temperature away from the chamber, the response of the viscoelastic crust becomes effectively elastic, satisfying equation (12) when r becomes sufficiently large: as shown in Figure S2, when r approaches $2r_o$, the elastic relation (12) becomes asymptotically true for forcing periods smaller than 10^6 days, with close to 0 phase shift between the displacement and stress, as well as a factor of -4μ between their amplitudes. Of course, our assumptions of radial symmetry break down at large spatial scales and long forcing periods (which effectively define a transition to crustal-scale isostatic response).

Assuming a sufficiently localized viscosity structure, we denote an effective ductile-brittle transition radius r_c for the magma chamber, such that for $r > r_c$, the response of the crust is elastic, and the solutions satisfy (12). The assumption that r_c resides in the model domain and is close to the chamber is required for the robustness of our method. Based on this assumption, the surface displacement can be obtained from the elastic stress at r_c, following a first order correction (Segall, 2010), namely

$$\hat{u}_z = -\frac{\hat{\sigma}_{rr}(r)r^3}{\mu}\frac{1}{d^2}(1-\nu)(\text{for } r > r_c). \tag{17}$$

We can verify that for a fully elastic domain ($Pr_o^3 = \sigma_{rr}r^3$ for all r), the surface displacement recovers the elastic counterpart (13).

Substituting equation (16) into (12) for $r > r_c$ reveals the value of the integral $\int_r^\infty \frac{r^3 dx}{x^4(K+\frac{4}{3}\mu^*(x))} = \frac{1}{3K+4\mu}$, which leads to invariant values within the effective elastic domain, given by

$$\hat{\sigma}_{rr} = \frac{C}{r^3}\frac{4\mu}{3K+4\mu}, \hat{u} = -\frac{C}{r^2}\frac{1}{3K+4\mu} \quad (\text{for } r > r_c). \tag{18}$$

Using the boundary condition at the reservoir wall $\hat{\sigma}_{rr}(r_o) = -\hat{P}$, and the precise solution to equation (16) for the whole domain, we find

$$\hat{P} = -\frac{C}{r_o^3}\left(1 - 3Kr_o^3 \int_{r_o}^\infty \frac{dx}{x^4(K+\frac{4}{3}\mu^*(x))}\right). \tag{19}$$

Hence, the relation between the stress in the effective elastic domain and the chamber pressure is

$$\hat{\sigma}(r) = -\frac{4\mu}{3K+4\mu}\frac{r_0^3}{r^3}\frac{\hat{P}}{1 - 3Kr_o^3 \int_{r_o}^\infty \frac{dr}{r^4(K+\frac{4}{3}\mu^*)}}, \text{for} \quad r > r_c, \tag{20}$$

which can be substituted into (17) to obtain the surface displacement $\hat{u}_z$, namely

$$\hat{u}_z = \frac{1-\nu}{\mu d^2}\hat{P}r_o^3 \frac{\frac{4\mu}{3K+4\mu}}{1 - \frac{3K}{3K+4\mu}\frac{r_o^3}{R_o^3} - 3Kr_o^3 \int_{r_o}^{R_o} \frac{dr}{r^4(K+\frac{4}{3}\mu^*)}}. \tag{21}$$

:

The transfer function between u_z and chamber overpressure is therefore

$$\mathcal{H}\{u_z|P\} = \frac{1-\nu}{\mu d^2}r_o^3 \frac{\frac{4\mu}{3K+4\mu}}{1 - \frac{3K}{3K+4\mu}\frac{r_o^3}{R_o^3} - 3Kr_o^3\int_{r_o}^{R_o}\frac{dr}{r^4(K+\frac{4}{3}\mu^*)}}. \tag{22}$$

In comparison with the elastic counterpart (14), we can define the normalized transfer function presented in main text equation (2) as

$$\bar{\mathcal{H}} = \frac{\{u_z|P\}}{\{u_z^{el}|P\}} = \frac{\frac{4\mu}{3K+4\mu}}{1 - 3Kr_o^3\int_{r_o}^{\infty}\frac{dr}{r^4(K+\frac{4}{3}\mu^*)}}. \tag{23}$$

The normalized transfer function is a correction based on the viscoelastic relaxation around the chamber on the elastic deformation generated by chamber pressurization

$$\hat{u}_z = \hat{u}_z^{el}\bar{\mathcal{H}}. \tag{24}$$

Expanding μ^* we can also express the normalized transfer function as the local Deborah number shown in the main text

$$\bar{\mathcal{H}} = \left(1 - 3r_o^3\int_{r_o}^{\infty}\frac{dr}{r^4\left(iDe(r)/\zeta + 1\right)}\right)^{-1} \tag{25}$$

where $\zeta = \frac{K}{K+\frac{4}{3}\mu}$.

Expanding the transfer function $\mathcal{H}$ using its amplitude and phase angle

$$\mathcal{H} = |\mathcal{H}|e^{i\varphi}$$

which corresponds to frequency-dependent amplitude $\mathcal{A} = |\mathcal{H}|$ and phase lag of $-\varphi$ reported in Figure 2 in the main text.

An effective discrete viscoelastic shell for variable coefficient problems

When the pressure forcing consists of a single frequency, the response of the viscoelastic space with non-uniform viscosity becomes identical to that of an elastic crust consisting of a discrete viscoelastic shell of uniform viscosity. The effective radius, temperature, viscosity,

and Deborah number in the uniform viscoelastic shell (shown in Figure 2 in the main text) are obtained via the following derivations.

Assume the effective system consists of a viscoelastic shell extending from r_o to R_{eff}, of uniform temperature T_{eff} corresponding to a uniform complex rigidity $\mu^{*,eff}$.

Integrating (9) across the effective shell, we find

$$\frac{\hat{u}(r_o)}{r_o} = \frac{\hat{u}(R_{eff})}{R_{eff}} - \frac{C}{3K + 4\mu^{*,eff}}\left(\frac{1}{r_o^3} - \frac{1}{R_{eff}^3}\right);$$

substituting this into the constitutive relation $\hat{\sigma}_{rr} = 3K\frac{\hat{u}}{r} + \frac{C}{r^3}$, the inner-shell boundary condition $\hat{\sigma_{rr}}(r_o) = -\hat{P}$, the elastic relation (12) at the outer shell boundary R_{eff}, we find the stress generated by the effective system measured at the shell's outer boundary is

$$\hat{\sigma}_{rr,eff}(R_{eff}) = -\hat{P}\frac{i\omega\tau_{eff} + \frac{3K}{3K+4\mu_c}}{i\omega\tau_{eff}\left(\frac{R_{eff}}{r_0}\right)^3 + \frac{3K}{3K+4\mu_c}}, \tag{26}$$

where $\tau_{eff} = \eta_{eff}/\mu$ is the effective (uniform) viscoelastic relaxation time in the shell with uniform viscosity η_{eff} and uniform temperature T_{eff}. Substituting (17) into (26), and comparing with the elastic solution (13) leads to

$$\hat{u}_{z,eff} = \mathcal{H}_{eff}\hat{u}_z^{el}, \tag{27}$$

where the transfer function $\mathcal{H}_{eff}(\omega)$ of the effective system consisting of a viscoelastic shell with relaxation time τ_{eff} and outer shell radius at R_{eff} is

$$\mathcal{H}_{eff}(\omega) = \frac{i\omega\tau_{eff} + \frac{3K}{3K+4\mu}}{i\omega\tau_{eff} + \left(\frac{r_o}{R_{eff}}\right)^3\frac{3K}{3K+4\mu}} = \frac{iDe_{eff} + \frac{3K}{3K+4\mu}}{iDe_{eff} + \left(\frac{r_o}{R_{eff}}\right)^3\frac{3K}{3K+4\mu}} = \frac{iDe_{rel} + R_{eff}^3/r_o^3}{iDe_{rel} + 1}, \tag{28}$$

where $De_{eff} = \omega\tau_{eff}$ is the uniform Deborah number in the shell, $De_{rel} = \frac{3K+4\mu}{3K}\omega\tau_{eff}R_{eff}^3/r_o^3$ is a Deborah number based on viscoelastic relaxation time for a uniform shell identified by (Dragoni & Magnanensi, 1989). The above relation (28) is used for finding the effective size (i.e., R_{eff}) and effective temperature of the viscoelastic shell, and the phase shift caused by

the effective transfer function shown in Figure 2 in the main text. The transfer function of the uniform shell sheds light on two rheological endmembers for the chamber+host rock system. The first is that of a purely elastic crust with viscoelastic shell thickness is 0, where $\mathcal{H}^{eff} = 1$ (no amplification, no phase delay). An elastic endmember is also reached when $\omega \to 0$, associated with full relaxation of stresses in the shell $r \leq R_{eff}$ (noting that $\hat{\sigma}_{rr,eff}(r = R_{eff}) = -\hat{P}$ in equation 26).

For the case of an increasing R_{eff}, the whole crust eventually becomes viscoelastic with uniform viscosity. The transfer function can be obtained through an analagous derivation, substituting the Laplace transform with the Fourier transform, as described in the next section. For fixed shell radius, the phase lag caused by the effective transfer function depends on the uniform Deborah number in the shell. Differentiating (28) with De_{eff} we obtain the maximum phase lag $\varphi_{max} = \tan^{-1}\left(\frac{1}{2} \left(\frac{R_{eff}}{r_o} \right)^{-3/2} \left(\frac{R_{eff}^3}{r_o^3} - 1 \right) \right)$, which is achieved when $De_{eff} = \zeta \left(\frac{R_{eff}}{r_o} \right)^{-3/2}$ with $\zeta = K/(K + 4/3\mu)$. As shown in Figure 2D this is associated with a phase lag less than the viscous fluid limit of $\pi/2$. In general De_{eff} and R_{eff} are coupled through ω so this formula does not hold precisely for the variable coefficient examples in the main text.

Transfer function for a viscoelastic crust with uniform viscosity

The transfer functions obtained in the previous two sections are based on the assumption that the crust becomes effectively elastic at sufficiently far distances from the chamber. Assuming that the crust is viscoelastic with uniform temperature, the complex rigidity becomes independent of radius. Earlier studies showed that the surface displacement in Laplace space for a viscoelastic crust can be obtained from the surface displacement of an elastic crust (13) via substituting the elastic constants by the complex rigidity and Poisson's ratio (Bonafede & Ferrari, 2009). We obtain the surface displacement of the viscoelastic crust (with uniform viscosity) in

Fourier space via substituting μ and ν in the elastic formula (13) with complex counterparts μ^* and $\nu^* = (3K - 2\mu^*)/(6K + 2\mu^*)$. Comparing the displacement $\hat{u}^{viscoel}$ for this special case with the elastic counterpart, we find the transfer function

$$\mathcal{H}\{u_z^{viscoel}|u_z^{el}\} = \frac{(iDe + 1)}{iDe} \frac{iDe + \frac{3K}{3K+4\mu}}{iDe + \frac{3K}{3K+\mu}}, \qquad (29)$$

which describes the correction to the elastic displacement by viscoelastic effects $\bar{\mathcal{H}}$ with uniform properties. The combination of (29) and the discrete transfer function (28) describe the response of a partially or fully viscoelastic crust with uniform viscosity. Equation (29) also corresponds to a physical scenario for the discrete shell system with an infinitely large viscoelastic shell. We can obtain from (29) a phase lag that monotonically increase with forcing period. When the forcing period is infinitely long, the phase lag becomes $\pi/2$, equivalent to the phase lag of a viscous fluid (Figure 2D in main text).

Viscous-elastic strain partitioning for the variable coefficient problem

In this section we show the steps for obtaining Fourier domain elastic and viscous components of the total deviatoric strain, and thus the spatial region where viscoelastic response occurs in the domain.

Maxwell viscoelastic rheology is

$$\frac{\sigma_{ij}^{dev}}{2\eta} + \frac{\dot{\sigma}_{ij}^{dev}}{2\mu} = \dot{\epsilon}_{ij}^{dev}, \qquad (30)$$

where the deviatoric strain and stress $\sigma_{ij}^{dev} = \sigma_{ij} - \frac{1}{3}Tr(\sigma_{ij})\delta_{ij}$, and the isotropic stress and strain satisfies $Tr(\sigma_{ij}) = 3KTr(\epsilon_{ij})$. In spherical coordinates with radial symmetry, the above relation is equivalent to (3). Observing (30) we can separate the total deviatoric strain rate $\dot{\epsilon}_{ij}^{dev}$ into a viscous part $\epsilon^{dev,viscous}$ and an elastic part $\epsilon^{dev,el}$ if the total deviatoric stress is known,

:

namely

$$\dot{\epsilon}_{rr}^{dev,viscous} = \sigma_{rr}^{dev}/2\eta, \qquad \dot{\epsilon}_{rr}^{dev,el} = \dot{\sigma}_{rr}^{dev}/2\mu. \tag{31}$$

With radial symmetry the deviatoric strain $\epsilon_{rr}^{dev} = \frac{2r}{3}\frac{d}{dr}\left(\frac{u}{r}\right)$. Substituting the Fourier transform of the above relation into the general solution (9), we find the Fourier transforms of the deviatoric strain and stress are given by

$$\hat{\epsilon}_{rr}^{dev} = \frac{C(\omega)}{\frac{3}{2}r^3(K + \frac{4}{3}\mu^*)}, \qquad \hat{\sigma}_{rr}^{dev} = 2\mu\frac{i\omega}{i\omega + \mu/\eta}\hat{\epsilon}_{rr}^{dev}, \tag{32}$$

where complex value C is the same shown in the general solution (16). The elastic and viscous components in the deviatoric strain are therefore

$$\hat{\epsilon}_{rr}^{dev,el} = \frac{i\omega}{i\omega + \mu/\eta}\hat{\epsilon}_{rr}^{dev}, \qquad \hat{\epsilon}_{rr}^{dev,viscous} = \frac{1}{i\omega\eta/\mu + 1}\hat{\epsilon}_{rr}^{dev}, \tag{33}$$

and the coefficient C can be obtained from applying the general solution (16) to the boundary condition of $\sigma_{rr}(r_o) = -P_{ch}$, namely

$$C(\omega) = -\frac{\hat{P}_{ch}}{1/r_o^3 - \int_{r_o}^{\infty}\frac{3K dr}{r^4(K + \frac{4}{3}\mu^*)}}. \tag{34}$$

For the special case of a monochromatic pressure forcing, the maximum total deviatoric strain and viscous deviatoric strain are obtained directly from observing (32) and (33):

$$\epsilon_{max}^{dev} = \frac{2|C(\omega)|}{3r^3|K + \frac{4}{3}\mu\frac{iDe}{iDe+1}|}, \quad \epsilon_{max}^{dev,viscous} = \frac{1}{|iDe + 1|}\frac{2|C(\omega)|}{3r^3|K + \frac{4}{3}\mu\frac{iDe}{iDe+1}|}, \tag{35}$$

where $De(r) = \omega\eta(r)/\mu$ is the r-dependent local Deborah number defined by the frequency of the forcing and the viscosity structure. We define the partition of the viscous strain by its ratio $\frac{\epsilon_{max}^{dev,viscous}}{\epsilon_{max}^{dev}} = \frac{1}{|iDe(r)+1|}$ and find that for an effective viscoelastic region defined by $\frac{\epsilon_{max}^{dev,viscous}}{\epsilon_{max}^{dev}} >= 10\%$, an effective boundary can be defined by the radius corresponding to local Deborah number $De \sim 10$, similar to the finding in Rucker et al. (2022).

For a broadband input of chamber pressure (e.g., square pulse), we calculate the solution for the strain components as function of radius and time using the inverse Fourier transform.

Combining (32) to (34), the Fourier transforms for the elastic deviatoric strain and viscous deviatoric strain are

$$\hat{\epsilon}_{rr}^{dev,el}(r,\omega) = \left(\frac{i\omega\tau}{i\omega\tau+1}\right)\frac{2C(\omega)}{3r^3(K+\frac{4}{3}\mu^*)}, \quad \hat{\epsilon}_{rr}^{dev,viscous}(r,\omega) = \left(\frac{1}{i\omega\tau+1}\right)\frac{2C(\omega)}{3r^3(K+\frac{4}{3}\mu^*)}.$$

$$(36)$$

The above solutions (36) in Fourier space are inverted to generate spatial-temporally resolved solutions on a grid with $\Delta r = 0.01r_o$. The time-maximum values for the strains are also obtained from (36), and the partition of the viscous strain extracted as a function of r, generating results in Figure 2b in the main text.

Text S2. Time domain solutions from transfer functions

The transfer functions identified in (23) allow for rapid computation of surface displacement in response to chamber pressure forcing that is a smooth function in time. In the main text we illustrate two examples: pressure forcing that is a square pulse in time, and pressure forcing that consists of repeated square pulses with varying duration and repose time in between the pulses. Obtaining the output time sequences demand a numerical scheme that a) computes the frequency spectra by applying the (discrete) Fourier transform on the input signal; b) modifies the frequency spectra based on the transfer function; and c) generates output signals by applying the inverse Fourier transform on the output frequency spectra. We implement these procedures using the symbolic toolbox of Matlab (2021b) (for integration and generating input signal) and Fourier transform codes (Carlos Adrian Vargas Aguilera (2022)).

It is worth noting that to compute the output time sequences, the frequency content for $\omega = 0$ is required. Because the zero-frequency component corresponds to a constant value in time, we account for this by assuming a zero displacement initial condition prior to chamber pressurization $u_z(t = 0^-) = 0$.

References

Bonafede, M., & Ferrari, C. (2009). Analytical models of deformation and residual gravity changes due to a mogi source in a viscoelastic medium. *Tectonophysics*, *471*(1), 4-13. Retrieved from `https://www.sciencedirect.com/science/article/pii/S0040195108004794` (Understanding stress and deformation in active volcanoes) doi: https://doi.org/10.1016/j.tecto.2008.10.006

Del Negro, C., Currenti, G., & Scandura, D. (2009). Temperature-dependent viscoelastic modeling of ground deformation: Application to etna volcano during the 1993–1997 inflation period. *Physics of the Earth and Planetary Interiors*, *172*(3), 299-309. Retrieved from `https://www.sciencedirect.com/science/article/pii/S0031920108003087` doi: https://doi.org/10.1016/j.pepi.2008.10.019

Dragoni, M., & Magnanensi, C. (1989). Displacement and stress produced by a pressurized, spherical magma chamber, surrounded by a viscoelastic shell. *Physics of the Earth and Planetary Interiors*, *56*(3), 316 - 328. Retrieved from `http://www.sciencedirect.com/science/article/pii/0031920189901660` doi: http://dx.doi.org/10.1016/0031-9201(89)90166-0

Fung, Y. C. (1965). *Foundations of solid mechanics* (2nd ed.). Prentice Hall.

McTigue, D. F. (1987). Elastic stress and deformation near a finite spherical magma body: Resolution of the point source paradox. *Journal of Geophysical Research: Solid Earth*, *92*(B12), 12931–12940. Retrieved from `http://dx.doi.org/10.1029/JB092iB12p12931` doi: 10.1029/JB092iB12p12931

Rucker, C., Erickson, B. A., Karlstrom, L., Lee, B., & J, G. (2022). A computational framework for time dependent deformation in viscoelastic magmatic systems. *in revision at Journal*

of Geophysical Research Solid Earth. doi: https://doi.org/10.31223/X5WH0N

Segall, P. (2010). *Earthquake and volcano deformation.* Princeton University Press. doi:
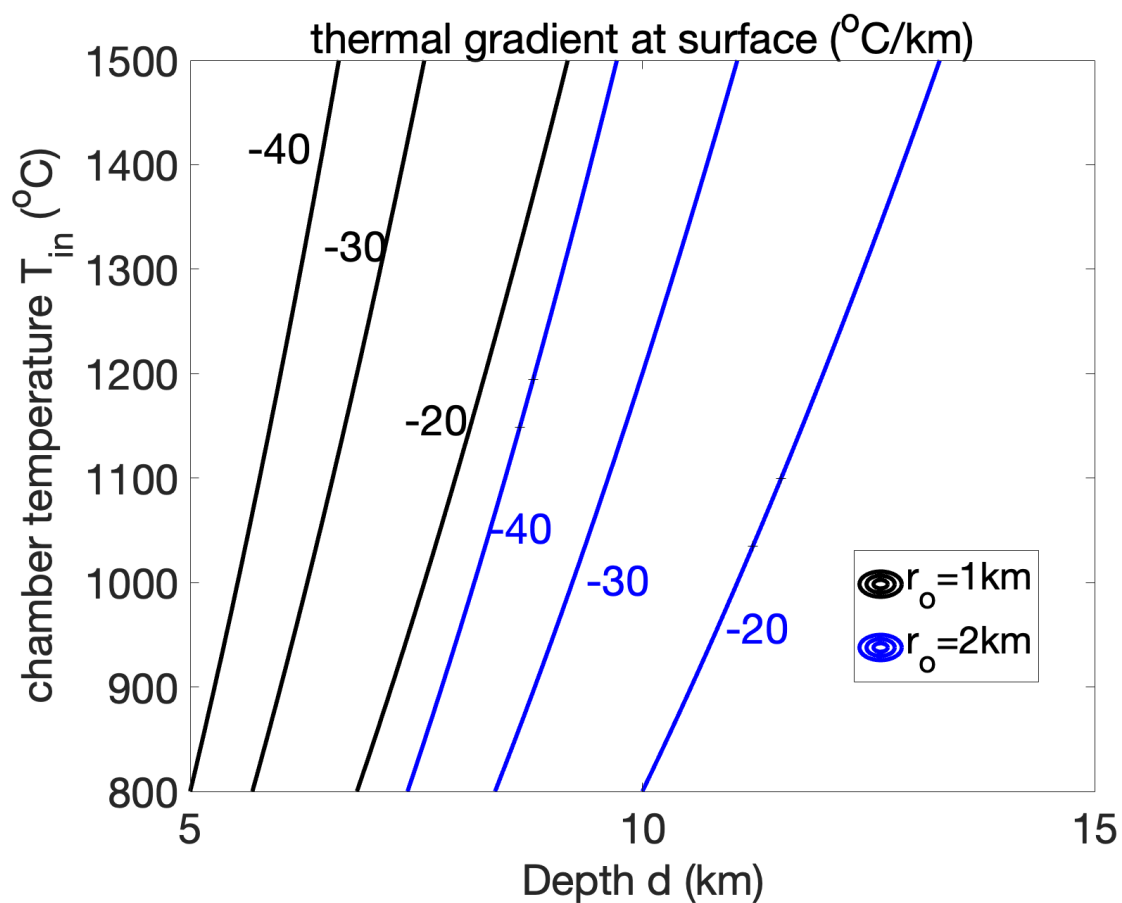
https://doi.org/10.1515/9781400833856

Figure S1. Contours of surface temperature gradient predicted by the radially symmetric

temperature solution shown for two different chamber radius (1km and 2km).

Table S1. Symbols of the constants used in the study

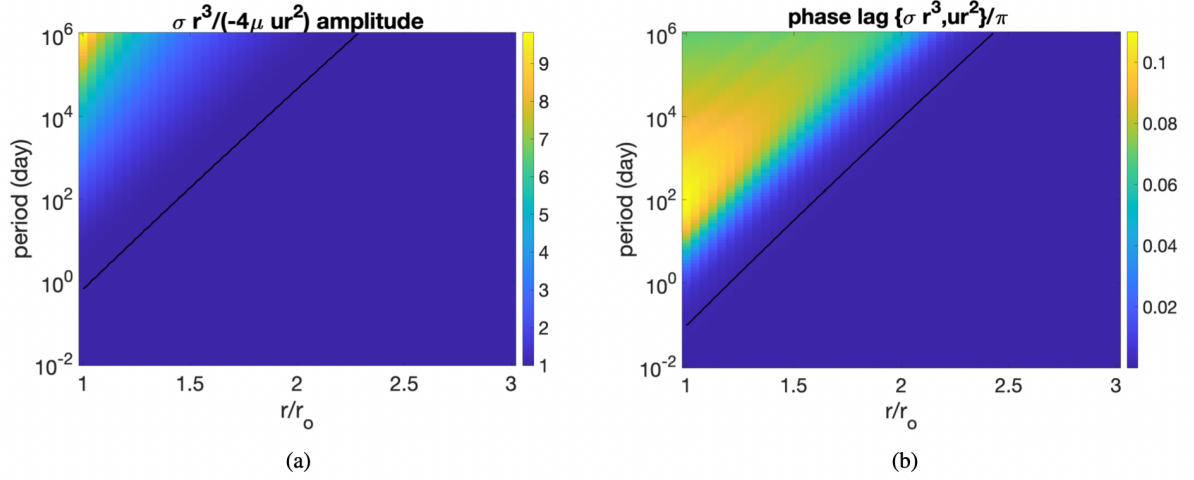|	symbol	definition	typical value/expression
constants	K	bulk modulus of crust	10GPa
	μ	shear modulus of crust	1Gpa
	ζ		$\frac{3K}{3K+4\mu}$
	T_{in}	magma chamber temperature	800-1200°C
	r_o	magma chamber radius	
	d	magma chamber depth	5-10r_o
	A_d	Dorn parameter	10^9 Pa.s
	E	activation energy	129KJ/mol
	R	Boltzmann constant	8.314 J/mol.K
	T	crust temperature	
	η	crust viscosity	$\eta = A_d e^{\frac{E}{RT}}$
	De	Deborah number	$\omega\eta/\mu$
variables	ω	forcing frequency	
	$\sigma_{rr,\theta\theta,\varphi\varphi}$	components of stress tensor	
	$\hat{\sigma}_{rr,\theta\theta,\varphi\varphi}$	Fourier transforms of stress components	
	u	crustal displacement	
	$\hat{u}$	Fourier transform of displacement $u(r,t)$	
	u_z	space-maximum surface vertical displacement	
	$\hat{u}_z$	Fourier transform of u_z	
	P	chamber pressure	
	$\hat{P}$	Fourier transform of chamber pressure	
	$\mathcal{H}\{f_{out}(t)|f_{in}(t)\}$	transfer function between the input quantity and output quantity	
	$\bar{\mathcal{H}}\{f_{out}(t)|f_{in}(t)\}$	transfer function normalized by the elastic limit	

(a)

(b)

Figure S2. Amplitude and phase lag between $\hat{\sigma}r^3$ and $-4\mu\hat{u}r^2$ calculated from (16) for a complex rigidity determined by $T_{in} = 1000^oC$, $\mu = 1GPa$, $K = 10GPa$, and depth $d = 5r_o$. According to equation (12), for an elastic domain the amplitude is 1 and phase lag is 0. Black lines indicate amplitude approximated as 1 and phase lag approximately at 0 (with 0.001 error).
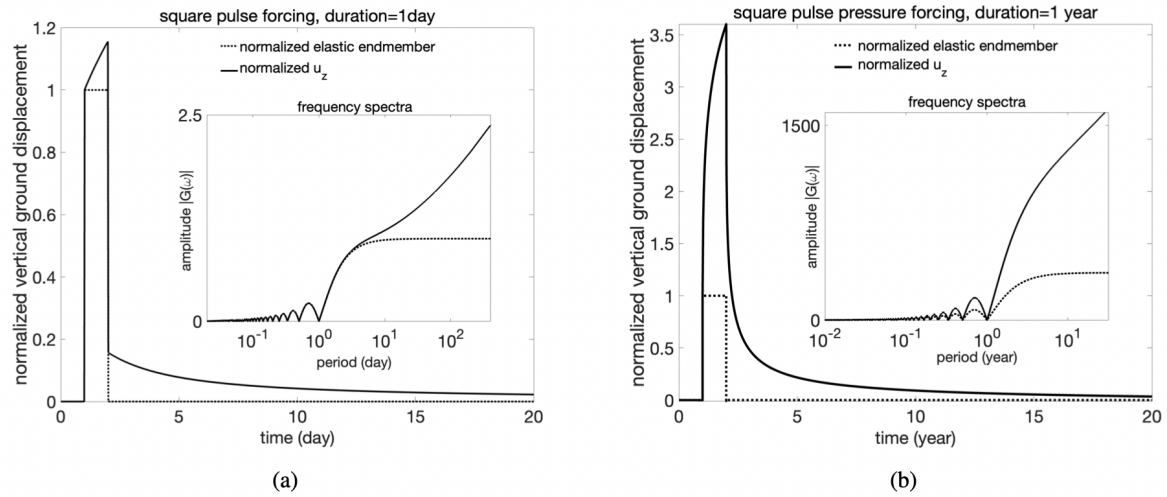
Figure S3. Additional results on surface displacements resulting from a square pulse pressure forcing of different durations. (a) shows the normalized vertical ground displacement and amplitude frequency spectra for a square pulse forcing with duration of 1 day. (b) shows ground displacement and frequency spectra for a square pulse forcing with duration of 1 year. A longer forcing duration results in higher viscoelastic amplification of the elastic displacement.
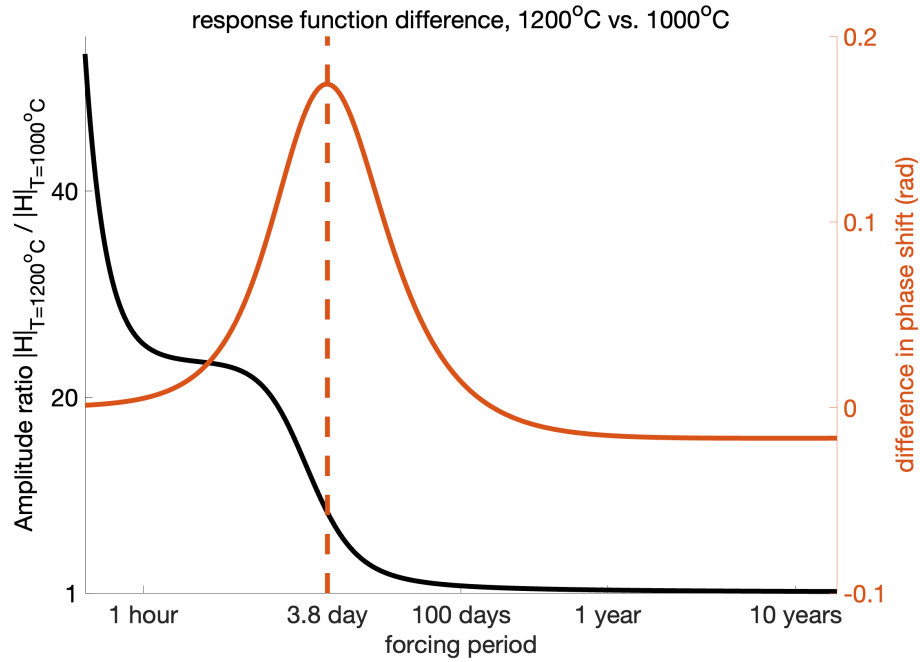
:

Figure S4. Difference between the transfer functions in amplitude and phase lags. The values for amplification and phase lags correspond to the results shown in main text Figure2 (a,b) for the two cases of different chamber temperatures: $d = 5r_o, 1000^oC$ and $d = 5r_o, 1200^oC$. Left axis (black) shows the ratio of the amplitude $|\mathcal{H}|$, where a value of 1 indicates that the two cases amplify the elastic displacement by the same amplification factor; a value larger than 1 indicates that the system with hotter temperature (1200^oC) amplify the input signal by a larger factor. Red curve (right axis) shows the difference between their phase shift angles ϕ; a positive value indicate that the hotter system has a larger phase delay. The result shows that the hotter system always amplifies the elastic displacement more strongly than the colder chamber for all frequency content. However, the hotter system has a larger phase delay for frequency content with periods smaller than 100 days, and for forcing signals with longer period, the colder system leads to more delay.
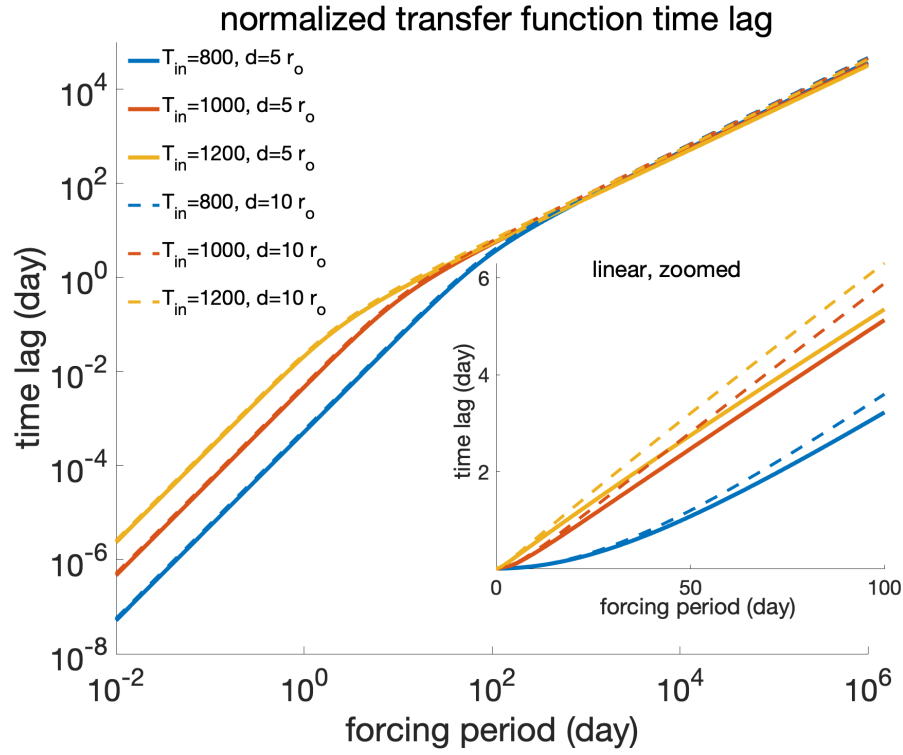
September 5, 2022, 5:09pm

Figure S5. Time lag of transfer functions as functions of forcing period/frequency. The time lags correspond to the phase lags φ shown in Figure2d in the main text with the relation of time lag $t_{lag} = \frac{\varphi}{\omega}$. The time-lags increase with increasing period. Insert shows the zoom in with linear scale.
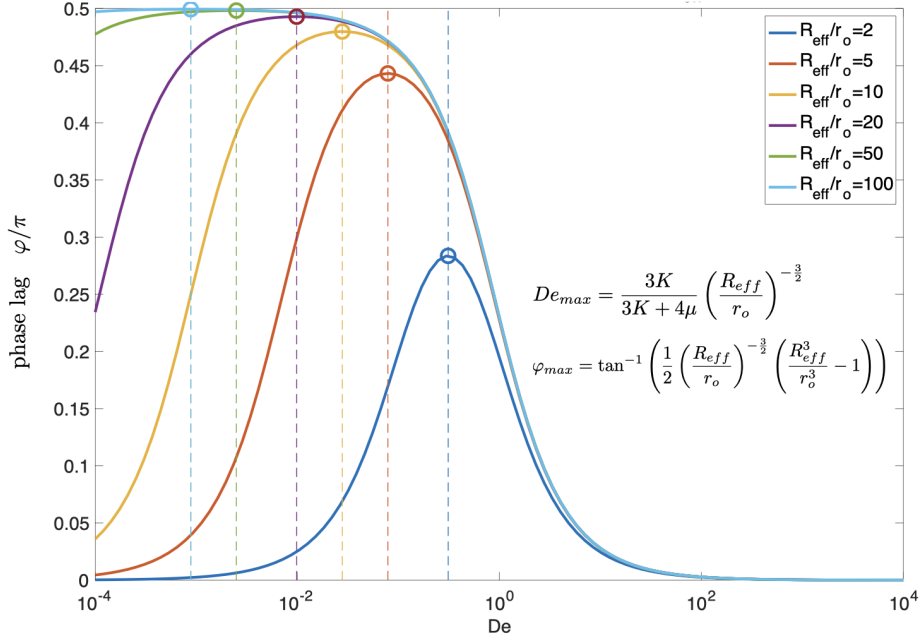
Figure S6. Phase lag of transfer function $\mathcal{H}_{eff}$ calculated according to (28) as function of uniform Debporah number for different viscous shell thickness R_{eff} (solid lines) for a system with $K = 10GPa, \mu = 1GPa$. The maximum phase lag is analytically predicted $\varphi_{max} = \tan^{-1}\left(\frac{1}{2}\left(\frac{R_{eff}}{r_o}\right)^{-3/2}\left(\frac{R_{eff}^3}{r_o^3} - 1\right)\right)$ with corresponding Deborah number $De_{max} = \frac{3K}{3K+4\mu}\left(R_{eff}/r_o\right)^{-3/2}$. Vertical dash-lines and circles show the location and value of the predicted maximum phase lag and De number, which coincide with the peaks of the curves.